Multivariate Amygdala Shape Modeling

University of Wisconsin-Madison

Department of Biostatistics and Medical Informatics

Technical Report 206

Moo K. Chung[a,b], **Keith J. Worsley**[d], **Brendon, M. Nacewicz**[b], **Kim M. Dalton**[b], **Richard J. Davidson**[b,c]

[a]Department of Biostatistics and Medical Informatics
[b]Waisman Laboratory for Brain Imaging and Behavior
[c]Department of Psychology and Psychiatry
University of Wisconsin, Madison, WI 53706, USA

[d]Department of Statistics
University of Chicago, Chicago, IL 60637, USA

December 13, 2008

Abstract

Although there are many imaging studies on traditional ROI-based amygdala volumetry, there are very few studies on modeling amygdala shape variations. This paper present a first unified computational and statistical framework for modeling amygdala shape variations in a clinical population. The recently developed weighted spherical harmonic representation is used as to parameterize, to smooth out, and to normalize amygdala surfaces. The complete amygdala surface modeling package AmygSurf used in the study is available at `www.stat.wisc.edu/∼mchung/research/amygdala`. The representation is subsequently used as an input for multivariate linear models accounting for age and brain size difference using SurfStat package (`galton.uchicago.edu/∼worsley`) that completely avoids the complexity of specifying design matrices. The methodology has been applied in detecting abnormal local shape variations in 22 high functioning autistic subjects. We have localized significant shape difference in autism in right amygdala. Further we have detected significant difference in interaction of shape and gaze fixation duration indicating localized abnormal

association of function and structure in autism.

Keywords: Amygdala, Spherical Harmonics, Fourier Analysis, Surface Flattening, General Linear Model

1. Introduction

Amygdala is an important brain substructure that has been implicated in abnormal functional impairment in autism (Dalton et al., 2005; Nacewicz et al., 2006; Rojas et al., 2000). Since the abnormal structure might be the cause of the functional impairment, there have been many studies on amygdala volumetry. However, previous amygdala volumetry results have been inconsistent. Aylward et al. (1999) and Pierce et al. (2001) reported that amygdala volume was significantly smaller in the autistic subjects while Howard et al. (2000) and Sparks et al. (2002) reported larger volume. Haznedar et al. (2000) and Nacewicz et al. (2006) found no volume difference. Schumann et al. (2004) reported that age dependent amygdala volume difference in autistic children and indicated that the age dependency to be the cause of discrepancy. All these previous studies traced the amygdalae manually and by counting the number of voxels within the region of interest (ROI), the total volume of the amygdala was estimated. The limitation of the traditional ROI-based volumetry is that it can not determine if the volume difference is diffuse over the whole ROI or localized within specific regions of the ROI (Chung et al., 2001). We present a novel computational and statistical framework that enables localized amygdala shape characterization and able to overcome the limitation of the ROI-based volumetry.

Although there are extensive literature on local cortical shape analysis (Chung et al., 2005; Fischl and Dale, 2000; Joshi et al., 1997; Taylor and Worsley, 2008; Thompson and Toga, 1996; Lerch and Evans, 2005; Luders et al., 2006; Miller et al., 2000), there are almost no literature on amygdala shape analysis other than Qiu et al. (2008). We hope to fill the gap and offer a new unified computational framework for analyzing amygdala shape. Our proposed framework utilizes the *weighted spherical harmonic representation* (Chung et al., 2007) for parameterization, surface smoothing and surface registration in a unified Hilbert space framework. We have developed the self contained MATLAB package called AmygSurf for performing weighted spherical harmonic representation (`www.stat.wisc.edu/~mchung/research/amygdala`).

Since the proposed representation technique requires a smooth mapping to a sphere, we have developed a new and very fast surface flattening technique based on the propagation of heat diffusion. By tracing the integral curve of heat gradient from a heat source (amygdala) to a heat sink (sphere), we can obtain the mapping. Since solving an isotropic heat equation in a 3D image volume is fairly straightforward, our proposed method offers a much simpler numerical implementation than surface flattening techniques such as conformal mappings (Angenent et al., 1999; Gu et al., 2004; Hurdal and Stephenson, 2004) quasi-isometric mappings (Timsari and Leahy, 2000) and area preserving mappings (Brechbuhler et al., 1995). The established spherical mapping is used to parameterize an amygdala surface using two Euler angles (φ, θ). The Euler angles serve as coordinates for representing amygdala surfaces using the weighted linear combination of spherical harmonics.

Our approach differ from previous spherical harmonic representation techniques (Gerig et al., 2001; Gu et al., 2004; Kelemen et al., 1999; Shen et al., 2004). The spherical harmonic representation has been mainly used a data reduction technique for compressing global shape features into small number of coefficients, and has been used to model various neuroanatomical structures such as ventricles (Gerig et al., 2001), hippocampi (Shen et al., 2004), cortical surfaces (Chung et al., 2007). The main geometric features are encoded in low degree coefficients while the noise will be in high degree spherical harmonics (Gu et al., 2004). Although the truncation of the series expansion can be viewed as a form of smoothing, there is no direct equivalence to the *full width at half maximum* (FWHM) usually associated with kernel smoothing. So it is difficult to relate the amount of smoothing associated the traditional spherical harmonic representation. Further the traditional series expansion suffers from the Gibbs phenomenon (ringing artifacts) (Chung et al., 2007; Gelb, 1997) that usually happens in trying to represent rapidly changing or discontinuous data with smooth periodic functions. To address theses issues, we have weighted the coefficients of the expansion exponentially such that the weights are related to heat kernel. The weighting has the effect of actually performing heat kernel smoothing (Chung et al., 2005). Hence, the amount of smoothing in the representation can be defined using the FWHM of the heat kernel so we have intuitive sense of how much smoothing we are performing before hand.

Once we obtain the weighted spherical harmonic representation of amygdalae, various multivariate tests were performed to detect the group difference between 22 autistic and 24 control subjects via the mulivariate linear modeling framework using the SurfStat package (`galton.uchicago.edu/∼worsley`). The SurfStat package offers a unified statistical analysis platform for various surface mesh data structures. The novelty of SurfStat package is that there is no need to specify design matrices that tend to baffle researchers not familiar with contrasts and design matrices. We will show various line by line codes that have been used for this study for illustration.

In summary, the methodological contributions of the paper are the introduction of a new unified computational framework for amygdala shape analysis and its MATLAB tool AmygSurf, and the introduction of a new multivariate linear modeling package SurfStat.

2. Image and Data Acquisition

High resolution T1-weighted magnetic resonance images (MRI) were acquired with a GE SIGNA 3-Tesla scanner with a quadrature head coil with 240 $\times$ 240 mm field of view and 124 axial sections. Details on image acquisition parameters are given in Dalton et al. (2005) and Nacewicz et al. (2006). T2-weighted images were used to smooth out inhomogeneities in the inversion recovery-prepared images using FSL (`www.fmrib.ox.ac.uk/fsl`). Total 22 autistic and 24 normal control MRI were acquired. Subjects were all males aged between 8 and 25 years. The Autism Diagnostic Interview-Revised (Lord et al., 1994) was used for diagnoses by trained researchers K.M. Dalton and B.M. Nacewicz (Dalton et al., 2005).

MRIs were first reoriented to the pathological plane for optimal comparison with anatomical atlases (Convit et al., 1999). Image contrast was matched by alignment of white and gray matter peaks on intensity histograms. Manual segmentation was done by a trained expert B.M. Nacewicz who has been blind to the diagnoses (Nacewicz et al., 2006). The manual segmentation also involves refinement through plane-by-palne comparison with ex vivo atlas sections (Mai et al., 1997). The reliability of the manual segmentation protocol was validated by two raters on 10 amygdale resulting in interclass correlation of 0.95 and the spatial reliability (intersection over union) average of 0.84. The total brain volume was also computed using an automated threshold-based connected voxel search method, and manually edited afterwards to ensure proper removal of skull, eye regions, brainstem and cerebellum. Figure 1 shows the manual segmentation of in three different cross sections. The amygdala (AMY) was traced in detail using various adjacent structures such as anterior commissure (AC), hippocampus (HIPP), inferior horn of lateral ventricle (IH), optic radiations (OR), optic tract (OT), temporal lobe white matter (TLWM) and tentorial notch (TN).

A subset of subjects (10 controls and 12 autistic) went through a face emotion recognition task consisting of showing 40 standardized pictures of posed facial expressions (8 each

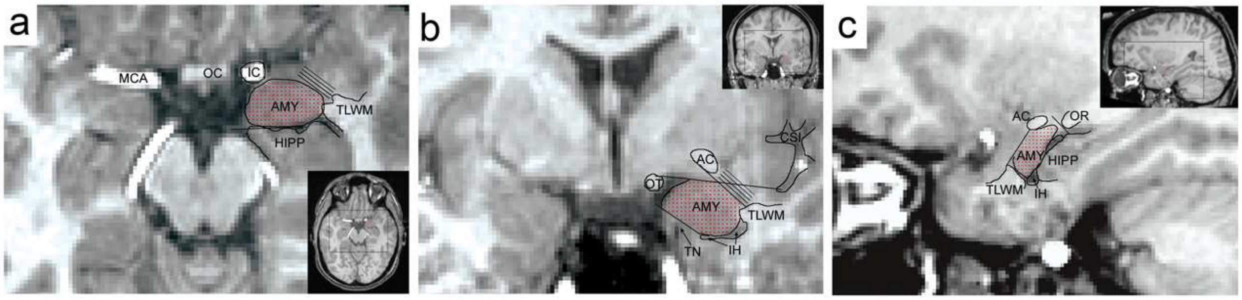

Figure 1. Amygdala manual segmentation at (a) axial (b) coronal and (c) midsagittal sections. The amygdala (AMY) was segmented using adjacent structures such as anterior commissure (AC), hippocampus (HIPP), inferior horn of lateral ventricle (IH), optic radiations (OR), optic tract (OT), temporal lobe white matter (TLWM) and tentorial notch (TN).

of happy, angry and sad, and 16 neutral) (Dalton et al., 2005). Subjects were required to press a button distinguishing neutral from emotional faces. The faces were black and white pictures taken from the Karolinska Directed Emotional Faces set (Lundqvist et al., 1998). The faces were presented using E-Prime software (`www.pstnet.com`) allowing for the measurement of response time for each trial. iView system with a remote eye-tracking device (SensoMotoric Instruments, `www.smivision.com`) was used at the same time to measure gaze fixation duration on eyes and faces during the task. The system records eye movements as the gaze position of the pupil over a certain length of time along with the amount of time spent on any given fixation point. It has been hypothesized that subjects with autism should exhibit diminished eye fixation duration relative to face fixation duration. If there is no confusion, we will simply refer *gaze fixation* as the ratio of durations fixed on eyes over faces. Note that this is a unitless measure. Our study enables us to show that abnormal gaze fixation duration is correlated with amygdala shape in spatially localized regions.

3. Amygdala Surface Parameterization

Once the amygdala binary segmentation $\mathcal{M}_a$ is obtained, the marching cubes algorithm (Sethian, 2002) was applied to obtain a triangle surface mesh $\partial\mathcal{M}_a$. The weighted spherical harmonic representation requires a smooth mapping from the surface mesh to a unit sphere S^2 to establish a coordinate system. We have developed a new surface flattening algorithm based on heat propagation.

We start with putting put a larger sphere $\mathcal{M}_s$ that encloses the amygala M_a (Figure 2).

The amygdala is assigned the value 1 while the enclosing sphere is assigned the value -1, i.e.

$$f(\mathcal{M}_a, \sigma) = 1 \text{ and } f(\mathcal{M}_s, \sigma) = -1 \tag{1}$$

for all $\sigma \in [0, \infty)$. The parameter σ is the diffusion time. The amygdala and the sphere serve as a heat source and a heat sink respectively. Then we solve isotropic diffusion

$$\frac{\partial f}{\partial \sigma} = \Delta f \tag{2}$$

with the given boundary condition (1). Δ is the 3D Laplacian. After sufficiently enough time, the solution reaches the heat equilibrium state where the additional diffusion does not make any change in heat distribution. The heat equilibrium state is also obtained by letting $\frac{\partial f}{\partial \sigma} = 0$ and solving for the Laplace equation

$$\Delta f = 0$$

with the same boundary condition. This will results in the equilibrium state denoted by $f(x, \sigma = \infty)$. Once we obtained the equilibrium state, we trace the path from the heat source to the heat sink for every mesh vertices on the isosurface of the amygdala using the gradient of the heat equilibrium $\nabla f(x, \infty)$. Similar formulation called the *Laplace equation method* has been used in estimating cortical thickness bounded by outer and inner cortical surfaces by establishing correspondence between two surfaces by tracing the gradient of the equilibrium state (Jones et al., 2006 ; Lerch and Evans, 2005). However, our approach is the first use of the same idea to surface flattening.

The heat gradients form vector fields originating at the heat source and ending at the heat sink (Figure 2). The integral curve of the gradient field at a mesh vertex $p \in \partial\mathcal{M}_a$ establishes a smooth mapping from the mesh vertex to the sphere. The integral curve τ is obtained by solving a system of differential equations

$$\frac{d\tau}{dt}(t) = \nabla f(\tau(t), \infty)$$

with $\tau(t = 0) = p$. The integral curve approach is a widely used formulation in tracking white matter fibers using diffusion tensors (Basser et al., 2000; Lazar and Alexander, 2003). These methods rely on discretizing the differential equations using the Runge-Kutta method ; however, the such computation intensive approach is not needed here. Instead of directly computing the gradient field $\nabla f(x, \infty)$, we computed the contours of the equilibrium state corresponding to the level set $f(x, \infty) = c$ for varying c between -1 and 1. The integral curve is then obtained by finding the shortest path from one contour to the next contour and connecting them together in a piecewise fashion. This is done in an iterative fashion as shown in Figure 2, where five contours corresponding to the values 0.6, 0.2, -0.2, -0.6, -1.0 are used to flatten the amygdala surface. Once we obtained the spherical mapping, we can then project the Euler angles (θ, φ) onto the amygdala surface and the Euler angles serve as the underlying parameterization for the weighted spherical harmonic representation.

4. Weighted Spherical Harmonic Representation

Reduction of Gibbs Phenomenon

The proposed *weighted spherical harmonic representation* fixes the Gibbs phenomenon (ringing effects) associated with the traditional Fourier descriptors and spherical harmonic representation (Brechbuhler et al., 1995; Gerig et al., 2001; Gu et al., 2004; Kelemen et al., 1999; Shen et al., 2004) by weighting the series expansion with exponential weights. The exponential weights make the representation converges faster and reduces the amount of ringing artifacts. Gibbs phenomenon (ringing artifacts) often arises in Fourier series expansion of discrete data. It is named after American physicist Josiah Willard Gibbs. In representing a piecewise continuously differentiable data using the Fourier series, the overshoot of the series happens at a jump discontinuity. The overshoot does not decease as the number of terms increases in the series expansion, and it converges to a finite limit called the Gibbs constant (Foster and Richard, 1991; Gelb, 1997). If surface coordinates are abruptly changing or their derivatives are discontinuous, the Gibbs phenomenon will severely distort the surface shape as shown in Figure 3, where a cube is reconstructed with various degree spherical harmonic representation but showing more ringing artifacts compared to the proposed weighted version.

The mesh coordinates for the amygdala surface $\partial\mathcal{M}_a$ is parameterized by the Euler angles $\Omega = (\theta, \varphi) \in [0, \pi] \otimes [0, 2\pi)$ as

$$p(\theta, \varphi) = (p_1(\theta, \varphi), p_2(\theta, \varphi), p_2(\theta, \varphi)).$$

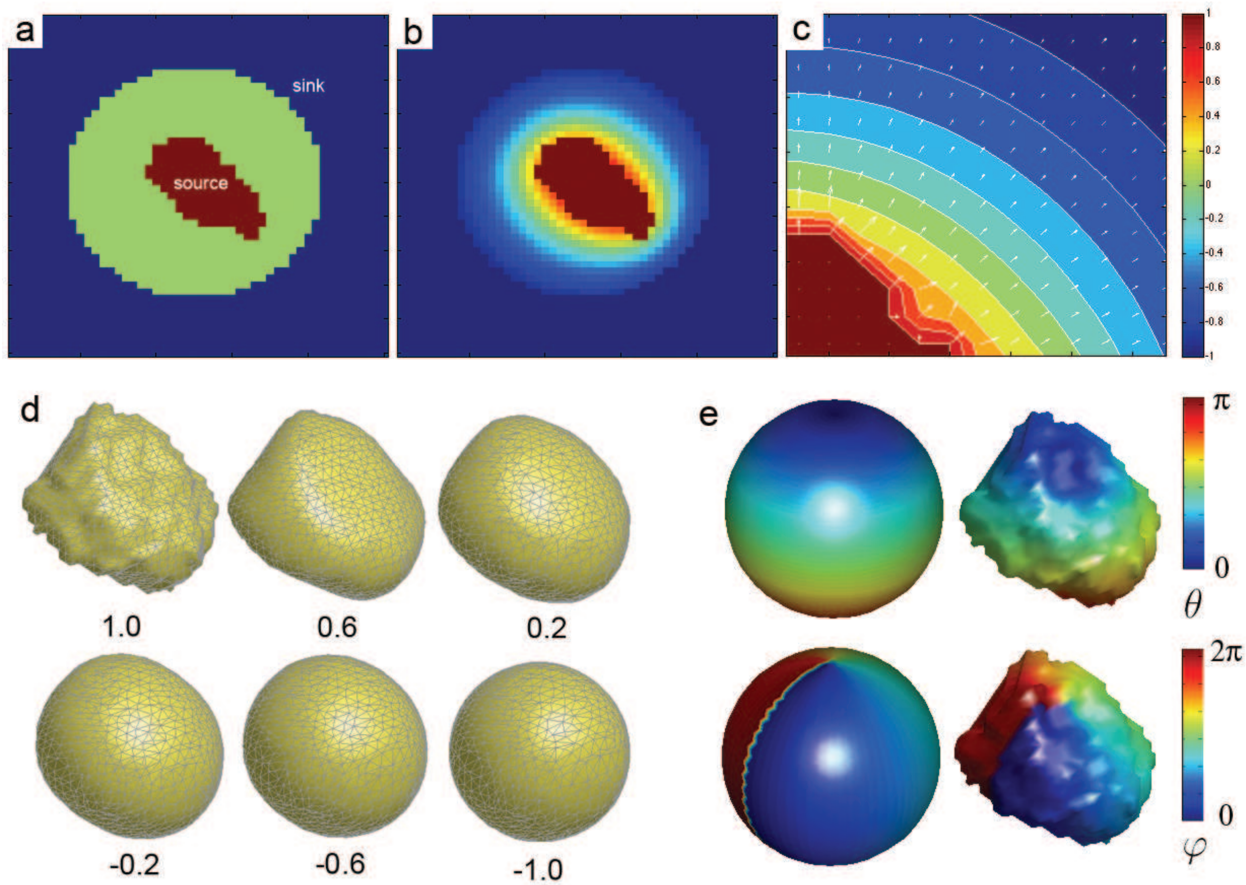

Figure 2. (a) The heat source (amygdala) is assigned value 1 while the heat sink is assigned the value -1. The diffusion equation is solved with these boundary condition. (b) After a sufficient number of diffusion, the equilibrium state $f(x, \infty)$ is reached. (c) The gradient field $\nabla f(x, \infty)$ shows the direction of heat propagation from the source to the sink. The integral curve of the gradient field is easily computed by connecting one level set to the next level sets of $f(x, \infty)$. (d) Amygala surface flattening is done by tracing the integral curve at each mesh vertex. The numbers $c = 1.0, 0.6, \cdots, -1.0$ corresponds to the level set $f(x, \infty) = c$. For amygdale, 5 to 10 contours are sufficient for flattening. (e) Amygdala surface parameterization using the Euler angles (θ, φ). The point $\theta = 0$ corresponds to the north pole of a unit sphere.

The weighted spherical harmonic representation is given by

$$p(\theta, \varphi) = \sum_{l=0}^{k} \sum_{m=-l}^{l} e^{-l(l+1)\sigma} f_{lm} Y_{lm}(\theta, \varphi),$$

where

$$f_{lm} = \int_{\theta=0}^{\pi} \int_{\varphi=0}^{2\pi} p(\theta, \varphi) Y_{lm}(\theta, \varphi)\ \sin\theta d\theta d\varphi$$

are the spherical harmonic coefficient vectors and Y_{lm} are spherical harmonics of degree l and order m defined as

$$Y_{lm} = \begin{cases} c_{lm} P_l^{|m|}(\cos\theta)\sin(|m|\varphi), & -l \le m \le -1, \\ \frac{c_{lm}}{\sqrt{2}} P_l^{|m|}(\cos\theta), & m = 0, \\ c_{lm} P_l^{|m|}(\cos\theta)\cos(|m|\varphi), & 1 \le m \le l, \end{cases}$$

where $c_{lm} = \sqrt{\frac{2l+1}{2\pi}\frac{(l-|m|)!}{(l+|m|)!}}$ and P_l^m is the *associated Legendre polynomial* of order m (Courant and Hilbert, 1953). The associated Legendre polynomial is given by

$$P_l^m(x) = \frac{(1-x^2)^{m/2}}{2^l l!} \frac{d^{l+m}}{dx^{l+m}} (x^2-1)^l,\ x \in [-1, 1].$$

The first few terms of the spherical harmonics are

$$Y_{00} = \frac{1}{\sqrt{4\pi}}, Y_{1,-1} = \sqrt{\frac{3}{4\pi}} \sin\theta \sin\varphi,$$
$$Y_{1,0} = \sqrt{\frac{3}{4\pi}} \cos\theta, Y_{1,1} = \sqrt{\frac{3}{4\pi}} \sin\theta\cos\varphi$$

and they are displayed in Figure 4. The coefficients f_{lm} are estimated in the least squares fashion (Chung et al., 2007; Gerig et al., 2001; Shen et al., 2004).

Connection to Heat Kernel Smoothing

One important property of the weighted spherical harmonic representation is that it is related to heat kernel smoothing, which is the differential geometric generalization of the traditional Gaussian kernel smoothing (Chung et al., 2005). On a unit sphere, the heat

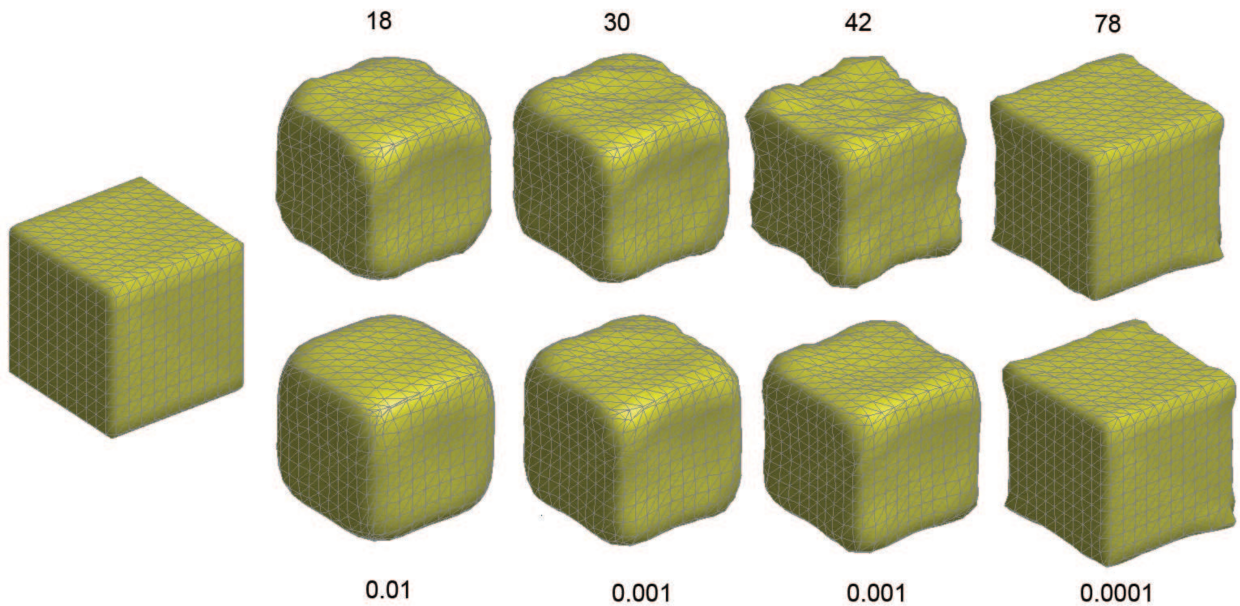

Figure 3. The first row shows the severe Gibbs phenomenon in the spherical harmonic representation of a cube for various degrees $k = 18, 30, 42, 78$. The second row is the weighted spherical harmonic representation at the same degree but with bandwidth $\sigma = 0, 01, 0.001, 0, 001, 0.0001$ respectively. In almost all degrees, the traditional spherical harmonic representation shows more prominent ringing artifacts compared to the proposed weighted version. The ringing artifacts is particularly severe for degree $k = 42$, and it also visually demonstrates the increased degree does not necessarily increase the accuracy of the spherical harmonic representation, possibly due to the discretization error.

kernel is defined as

$$K_\sigma(\Omega, \Omega') = \sum_{l=0}^{\infty} \sum_{m=-l}^{l} e^{-l(l+1)\sigma} Y_{lm}(\Omega) Y_{lm}(\Omega'). \tag{3}$$

The heat kernel is symmetric and positive definite, and a probability distribution so that

$$\int_{S^2} K_\sigma(\Omega, \Omega')\, d\mu(\Omega) = 1.$$

The *bandwidth* σ controls the dispersion of the kernel and as $\sigma \to 0$, the kernel becomes the Dirac-delta function, i.e.

$$\lim_{\sigma \to 0} K_\sigma(\Omega, \Omega') = \delta(\Omega - \Omega').$$

However, this is where the similarity with the traditional Gaussian kernel ends. Since the heat kernel flattens out as $\sigma \to \infty$ while it has to integrate to unity, we must have

$$\lim_{\sigma \to \infty} K_\sigma(\Omega, \Omega') = \frac{1}{4\pi}.$$

We define *heat kernel smoothing* of coordinates p as the convolution

$$K_\sigma * p(\Omega) = \int_{S^2} K_\sigma(\Omega, \Omega') p(\Omega')\, d\mu(\Omega'). \tag{4}$$

By substituting (3) into equation (4) and rearranging the integral with the summation, we can show that heat kernel smoothing is identical to the weighted spherical harmonic representation:

$$K_\sigma * f(\Omega) = \sum_{l=0}^{\infty} \sum_{m=-l}^{l} e^{-l(l+1)\sigma} \langle f, Y_{lm} \rangle Y_{lm}(\Omega), \tag{5}$$

Hence, the weighted Fourier representation should inherit all the properties of kernel-based smoothing.

Surface Normalization and Resampling

Once amygdala surfaces are represented with weighted spherical harmonics, we need to establish surface correspondence across different surfaces for later statistical analysis. However, it is computationally difficult to establish the correspondence across different amygdala

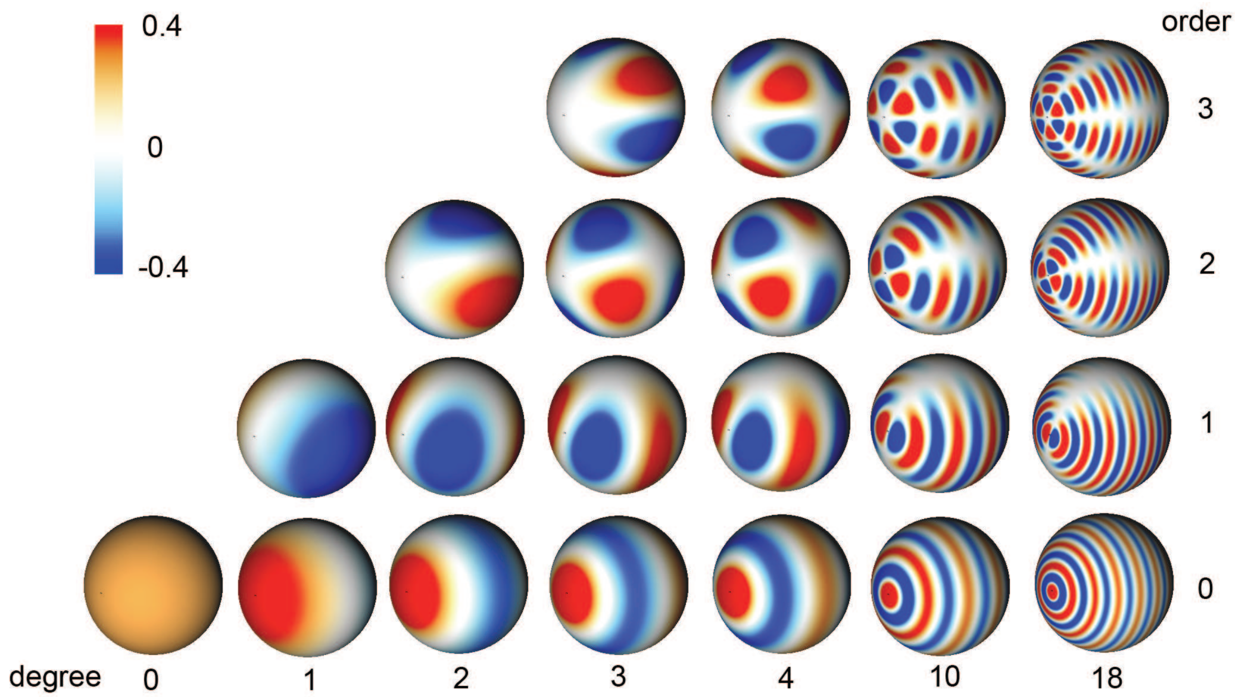

Figure 4. Spherical harmonic basis for various degree and order. Only nonnegative orders are shown. For the l-th degree, there are $2l + 1$ different orders. The spherical harmonic representation construct a function defined on a sphere as a linear combination of this basis.

meshes since any two triangle meshes will have different topology and connectivity. For instance, the first amygdala surface in Figure 5-(a) has 1270 vertices and 2536 faces while the second surface has 1302 vertices and 2600 faces. The proposed weighted spherical harmonic representation can establish correspondence between topologically different meshes. The correspondence is established by matching the coefficient of spherical harmonics at the same degree and order. This correspondence is optimal in the least squares sense (Chung et al., 2007).

Denote the surface coordinates corresponding to the i-th subject as p^i. Then we have the weighted spherical harmonic representation

$$p^i(\Omega) = \sum_{l=0}^{k} \sum_{m=-l}^{l} e^{-l(l+1)\sigma} f_{lm}^i Y_{lm}(\Omega), \tag{6}$$

where f_{lm}^i are the spherical harmonic coefficient vector. There are total $(k+1)^2 \times 3$ coefficients to be estimated in the least squares fashion. Since the representation is continuously defined in any $\Omega \in [0, \pi] \otimes [0, 2\pi)$, it is possible to resample the amygdala meshes using a topologically different spherical mesh. We have uniformly sampled the unit sphere and constructed a spherical mesh with 2563 vertices and 5120 faces. This spherical mesh serves as a common mesh topology for all amygdala surfaces. After the resampling, all amygdala surface will have the identical mesh topology as the spherical mesh, and the identical vertex indices will correspond across different surfaces (Figure 5-(c)). The idea of uniform mesh topology has been previously used in the basis of MNI cortical mesh normalization (Chung et al., 2005; MacDonald et al., 2000).

The proposed idea of surface normalization and resampling can be used to construct the average amygdala surface. We assume there are total n surfaces. The average surface $\overline{p}$ is given as

$$\overline{p} = \frac{1}{n} \sum_{i=1}^{n} \sum_{l=0}^{k} \sum_{m=-l}^{l} e^{-l(l+1)\sigma} f_{lm}^i Y_{lm}. \tag{7}$$

The average left and right amygdala templates are constructed by averaging the spherical harmonic coefficients of all 24 control subjects. The template surfaces serve as the reference coordinates for projecting the subsequent statistical parametric maps (Figure 7-8).

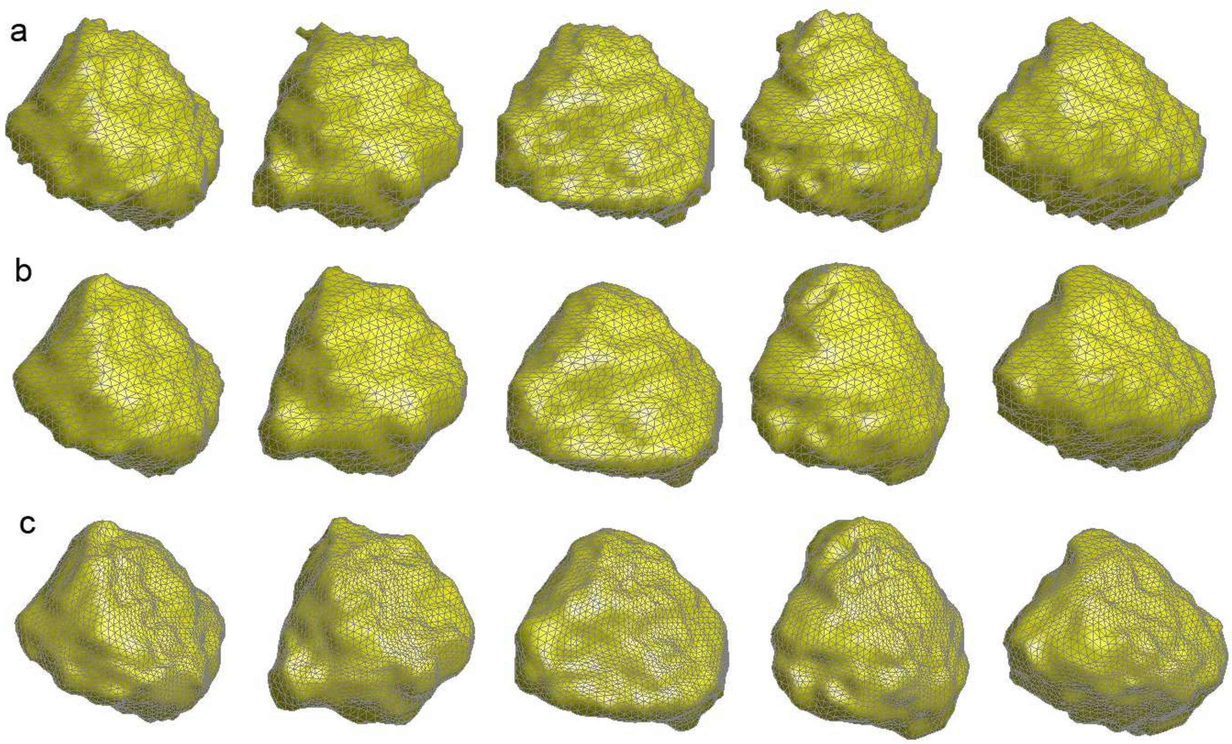

Figure 5. (a) Five representative left amygdala surfaces. (b) 42 degree weighted spherical harmonic representation. Surfaces have different mesh topology. (c) However, meshes can be resampled in such a way that all meshes have identical topology with exactly 2562 vertices and 5120 faces. Identically indexed mesh vertices correspond across different surfaces in the least squares fashion.

Degree Selection

Since it is impractical to sum the representation all the way up to $k \to \infty$, we need a rule for truncating the series expansion. Given the bandwidth of heat kernel, we automatically determine if increasing degree k has any effect on the goodness of the fit of the representation. In all spherical harmolnic literature (Gerig et al., 2004; Gerig et al., 2001 ; Gu et al., 2004; Shen and Chung, 2006; Shen et al., 2004), the truncation degree is simply selected based on a pre-specified error bound that depends on the size of anatomical structure. Our proposed statistical framework does not depend on the size of anatomical structures.

Although increasing the degree increases the goodness-of-fit of the representation, it also increases the number of coefficients to be estimated quadratically. It is necessary to find the optimal degree where the goodness-of-fit and the number of parameters balance out. Consider the following k-th degree reconstruction error model:

$$p(\Omega_i) = \sum_{l=0}^{k-1} \sum_{m=-l}^{l} e^{-l(l+1)\sigma} f_{lm} Y_{lm}(\Omega_i) + \sum_{m=-k}^{k} e^{-k(k+1)\sigma} f_{km} Y_{km}(\Omega_i) + \epsilon(\Omega_i) \tag{8}$$

at each mesh vertex Ω_i with a zero mean Gaussian noise. We test if adding the k-th degree terms to the $k-1$-th degree model is statistically significant by formally testing

$$H_0 : f_{k,-k} = \cdots = f_{k,k} = 0.$$

Let E_0 be the sum of squared residual corresponding to the reduced model while E be that of the full model. Under H_0, the test statistic is the F statistic

$$F = \frac{(E_0 - E)/(2k+1)}{E_0/(n-(k+1)^2)}$$

which is distributed as the F-distribution with $2k+1$ and $n-(k+1)^2$ degrees of freedom. At each degree, we compute the corresponding p-value and stop increasing the degree if it is smaller than pre-specified significance $\alpha = 0.01$. For bandwidths $\sigma = 0.01, 0.001, 0.0001$, the approximate optimal degrees are 18, 42 and 78 respectively. In our study, we have used $k = 42$ degree representation corresponding to bandwidth $\sigma = 0.001$. The bandwidth 0.01 smoothes out too much local details while the bandwidth 0.0001 introduces too much voxel discretization error into the representation.

AmygSurf

AmygSurf package (`www.stat.wisc.edu/~mchung/research/amygdala`) is developed by M.K. Chung to perform the weighted spherical harmonic representation from binary amygdala segmentation. Given an amygdala mesh `surf`, which is, for instance, given as a structure array of the form

```
>surf
surf =
    vertices: [1270x3 double]
       faces: [2536x3 double]
```

The amygdala flattening algorithm in AmygSurf will generate the corresponding unit sphere mesh `sphere` that has identical topology as `surf`. The weighted spherical harmonic representation `P` with degree $k = 42$ and the bandwidth $\sigma = 0.001$ is computed by running

```
>[P,coeff]=SPHARMsmooth(surf,sphere,42,0.001);
```

The detailed step-by-step MATLAB command line instructions are given in the website. The package also contains few modification of SurfStat for amygdala specific data manipulation and visualization. Along with SurfStat, AmygSurf is all we need to analyze amygdala surfaces presented in the result section.

5. Multivariate Linear Models

Multivariate linear models (Anderson, 1984; Taylor and Worsley, 2008; Worsley et al., 2004) generalize widely used univariate general linear models (Worsley et al., 1996) by incorporating vector valued response and explanatory variables. The weighted spherical harmonic representation of amygdala surface coordinates will be taken as the response variable. Consider the following multivariate linear model at each fixed (θ, φ)

$$P_{n\times 3} = X_{n\times p}B_{p\times 3} + Z_{n\times r}G_{r\times 3} + U_{n\times 3}\Sigma_{3\times 3}, \tag{9}$$

where $P = (p^{1\prime}, p^{2\prime}, \cdots, p^{n\prime})'$ is the matrix of weighted spherical harmonic representation, X is the matrix of contrasted explanatory variables, and B is the matrix of unknown coefficients. Nuisance covariates are in the matrix Z and the corresponding coefficients are in the matrix

G. The subscripts denote the dimension of matrices. The components of Gaussian random matrix U are zero mean and unit variance. Σ accounts for the covariance structure of coordinates. Then we are interested in testing the null hypothesis

$$H_0 : B = 0.$$

For the reduced model corresponding to $B = 0$, the least squares estimator of G is given by

$$\widehat{G}_0 = (Z'Z)^{-1}Z'P.$$

The residual sum of squares of the reduced model is

$$E_0 = (P - Z\widehat{G}_0)'(P - Z\widehat{G}_0)$$

while that of the full model is

$$E = (P - X\widehat{B} - Z\widehat{G})'(P - X\widehat{B} - Z\widehat{G}).$$

Note that $\widehat{G}$ is different from $\widehat{G}_0$ and estimated directly from the full model. By comparing how large the residual E is against the residual E_0, we can determine the significance of coefficients B. However, since E and E_0 are matrices, we take a function of eigenvalues of EE_0^{-1} as a statistic. For instance, *Lawley-Hotelling trace* is given by the sum of eigenvalues while *Roy's maximum root* R is the largest eigenvalue. In the case there is only one eigenvalue, all these multivariate test statistics simplify to *Hotelling's T-sqaure* statistic. The Hotelling's T-square statistic has been widely used in modeling 3D coordinates and deformations in brain imaging (Cao and Worsley, 1999; Chung et al., 2001; Gaser et al., 1999; Joshi, 1998; Thompson et al., 1997). The random field theory for Hotelling's T-square statistic has been available for a while (Cao and Worsley, 1999). However, the random field theory for the Roy's maximum root has not been developed until recently (Taylor and Worsley, 2008; Worsley et al., 2004). This paper is the first few that utilizes the result originally developed in Worsley et al. (2004).

The inference for Roy's maximum root is based on the Roy's union-intersection principle (Roy, 1953), which simplifies the multivariate problem to a univariate linear model. Let us multiply an arbitrary constant vector $\nu_{3\times 1}$ on both sides of (9):

$$P\nu = XB\nu + ZG\nu + U\Sigma\nu. \tag{10}$$

Obviously (10) is a usual univariate linear model with a Gaussian noise. For the univariate testing on $B\nu = 0$, the inference is based on the F statistic with p and $n-p-r$ degrees of freedom, denoted as F_ν. Then Roy's maximum root statistic can be defined as $R = \max_\nu F_\nu$. Now it is obvious that the usual random field theory can be applied in correcting for multiple comparisons. The only trick is to increase the search space, in which we take the supreme of the F random field, from the amygdala template surface to much higher dimension to account for maximizing over ν as well.

SurfStat

SurfStat package (`galton.uchicago.edu/~worsley`) is developed by K.J. Worsly utilizing a model formula and avoids the explicit use of design matrices and contrasts, which tend to be a hinderance to most end users not familiar with such concepts. SurtStat can import MNI (MacDonald et al., 2000) and FreeSurfer (`surfer.nmr.mgh.harvard.edu`) based cortical mesh formats. The model formula approach is implemented in many statistics packages such as Splus (`www.insightful.com`) R (`www.r-project.org`) and SAS (`www.sas.com`). These statistics packages accept a linear model like

$$\texttt{P} = \texttt{Group} + \texttt{Age} + \texttt{Brain}$$

as the direct input for linear modeling avoiding the need to explicitly state the design matrix. `P` is a $n \times 3$ matrix of coordinates of weighted spherical harmonic representation, `Age` is the age of subjects, `Brain` is the total brain volume of subject and `Group` is the categorical group variable (0=control, 1 = autism). This type of model formula has yet to be implemented in SPM (`www.fil.ion.ucl.ac.uk/spm`) or AFNI (`afni.nimh.nih.gov`) packages.

We show few SurfStat MATLAB command lines to illustrate how the multivariate linear modeling is done. To test the effect of `Group` variable on the representation `P`, we run

```
>E0 = SurfStatLinMod(P,1);
>E = SurfStatLinMod(P,1+Group,Avg);
>LM = SurfStatF(E,E0);
```

`Avg` is the weighted spherical harmonic representation of the average amygdala surface. The variable `E0` contains the information about the sum of squared residual of the reduced model `P=1` while `E` contains that of the full model `P = 1 + Group`. Based on the sum of squared residuals, `LM` computes the F-statistics. The F statistic value is stored in `LM.t`. To display the F statistic value is on top of the average surface, we use `FigureOrigami(Avg,LM.t)`, which is the part of the AmygSurf package (Figure 7). To determine the random field based thresholding corresponding to $\alpha = 0.1$ level, we run

```
>resels = SurfStatResels(LM);
>stat_threshold( resels, length(LM.t),1,LM.df,0.1,[],[],[],LM.k)
peak_threshold =
   26.9918
```

`resels` computes the resels of the random field and `peak_threshold` is the threshold corresponding to 0.1 level. We can construct a more complicated model that includes the brain size and age variables.

```
>E0 = SurfStatLinMod(P,Age+Brain);
>E = SurfStatLinMod(P,Age+Brain+Group,Avg);
>LM = SurfStatF(E,E0);
```

To see if gaze fixation `Fixation` correlates differently with surface coordinates `P` between the groups, we run

```
>E0=SurfStatLinMod(P,Age+Brai +Group+Fixation);
>E=SurfStatLinMod(P,Age+Brain+Group+Fixation+Group*Fixation,Avg);
>LM=SurfStatF(E,E0);
```

6. Results

Amygdala Volumetry

We have counted the number of voxels in amygdala segmentation and computed the volume of both left and right amygdale. The volumes for control subjects ($n = 22$) are left $1892 \pm 173\text{mm}^3$, right $1883 \pm 171\text{mm}^3$. The volumes for autistic subjects ($n = 24$) are left $1858 \pm$

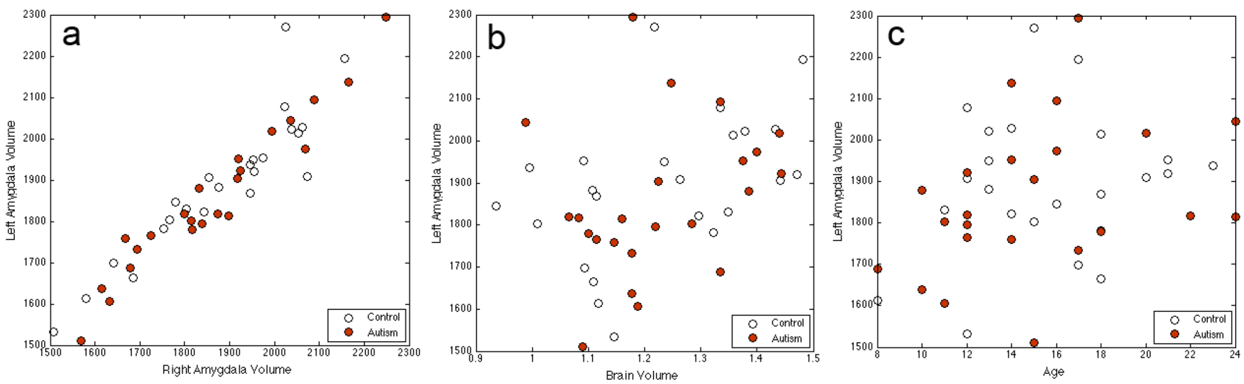

Figure 6. Scatter plots of left amygdala volume (vertical axis) vs. (a) right amygdala volume (b) total brain volume and (c) age showing significant confounding effect of total brain volume and age on amygdala volume. Any statistical analysis on amygdala volume and shape needs to account for brain volume and age.

182mm^3, right 1862$\pm$181mm^3. The volume difference between the groups are not statistically significant based on the two sample t-test ($p = 0.52$ for left and 0.69 for right). Literature report somewhat contradicting results (Aylward et al., 1999; Haznedar et al., 2000; Nacewicz et al., 2006; Pierce et al., 2001; Schumann et al., 2004; Sparks et al., 2002). Previous amygdala volumetry studies have been inconsistent. Aylward et al. (1999) and Pierce et al. (2001) reported that significantly smaller amygdala volume in the autistic subjects while Howard et al. (2000) and Sparks et al. (2002) reported larger volume. Haznedar et al. (2000) and Nacewicz et al. (2006) found no volume difference. These inconsistency might be due to the lack of control for brain size and age in statistical analysis (Schumann et al., 2004). The effect of age and the total brain volume on amygdala volume can be seen in Figure 6. Therefore, it is necessary to test group difference while accounting for the total brain volume and age. We did not detect any group difference in amygdala volume for both left ($p = 0.66$) and right ($p = 0.53$) amygdale. The testing was done using SurfStat.

Local Shape Difference

From the amygdala volumetry result, it is still not clear if shape difference might be still present within amygdala. It is possible to have no significant volume difference while having shape difference. So we have performed multivariate linear modeling on the weighted spherical harmonic representation. We have tested the effect of group variable by comparing the sum of squared residuals of the full (`P=1+Group`) and the reduced (`P=1`) models, which resulted in the threshold of 26.99, which is far larger than the maximum F statistic value of 13.55 in Figure 7 (a). So we could not detect any shape difference in the left amygdala. For the right amygdala, the $\alpha = 0.1$ level thresholding is 26.64 which is far larger than the maximum F statistic value of 12.11. So again there is no statistically significant shape difference in the right amygdala.

Local Shape Difference Accounting for Age and Brain Size

We have tested the effect of `Group` variable while accounting for age and the total brain volume by comparing the sum of squared residuals of the full (`P=Age+Brain+Group`) and the reduced (`P=Age+Brain`) models. The maximum F statistics are 14.77 (left) and 12.91 (right) while the threshold corresponding to $p = 0.1$ is 14.58 (left) and 14.61 (right). Hence, we still did not detect group difference in the right amygdala (Figure 7-c) while there is a localize region of group difference in the left amygdala (Figure 7-d). By computing the average surface coordinate difference (autism - control), we have determined the direction of shape difference. See the vector fields of the enlarged area in Figure . The outward direction implies that the autistic subjects has larger amygdale in the region.

Brain and Behavior Association

Among total 46 subjects, 10 control and 12 autistic subjects went through face emotion recognition task and gaze fixation `Fixation` was observed. The gaze fixation are 0.30 ± 0.17 (control) and 0.18 ± 0.16 (autism), which differ statistically ($p = 0.11$). Nacewicz et al. (2006) showed the gaze fixation duration correlate differently with amygdala volume between the two groups; however, it is not clear if the association difference is local or diffuse over all amygdala. So we have tested the significance of the interaction between `Group` and `Fixation` in the multivariate linear model. We have obtained regions of significant interaction in the both left ($p < 0.05$) and right ($p < 0.02$) amygdale (Figure 8). The largest cluster in the right amygdala shows highly significant interaction ($\max F = 65.68$, $p = 0.003$). The color bar in Figure 8-(b) has been thresholded at 40 for better visualization. The scatter plots of x, y and z coordinates vs. `Fixation` are shown at the two most significant clusters in each amygdala. The first row is for autism while the second row is for control subjects. The red lines are linear regression lines. The significance of interaction implies difference in regression slopes between groups in a multivariate fashion. Note that there are three different slopes corresponding to x, y and z coordinates.

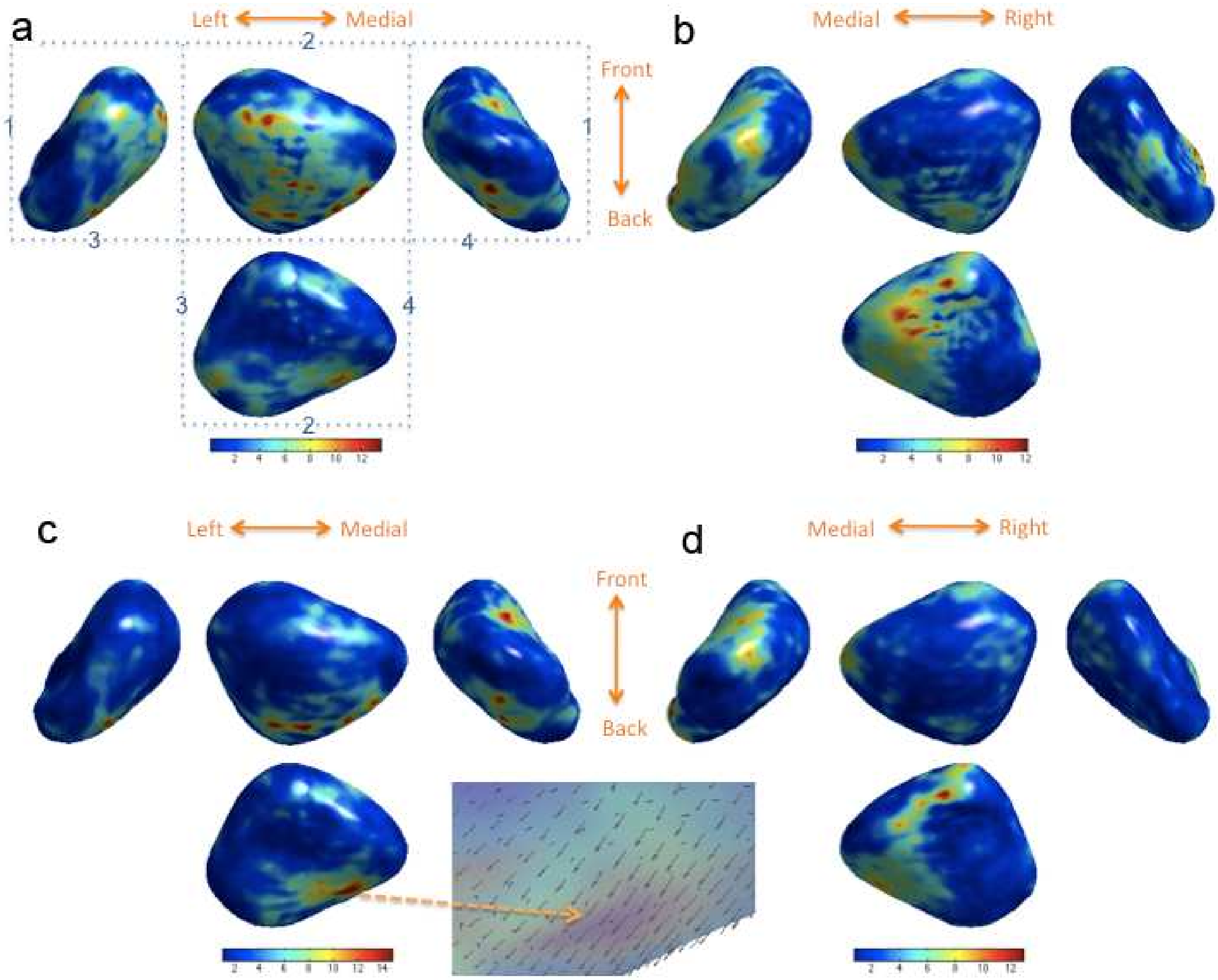

Figure 7. F statistic map of shape difference displayed on the average left amygdala (a) and right amygdala (b). We did not detect any significant difference ($p < 0.01$). The left amygdala (a) is displayed in such a way that, if we fold along the dotted lines and connect the identically numbered lines, we obtain the 3D view of the amygdala. The top middle rectangle corresponds to the axial view obtained by observing the amygdala from the top of the brain. (c) and (d) shows the F statistic map of shape difference accounting for age and the total brain volume. We have detected regions of shape difference in the left amygdala (red regions) ($p < 0.1$). The arrows in the enlarged area show the direction of shape difference (autism - control) indicating autistic subjects has larger amygdala in that area.

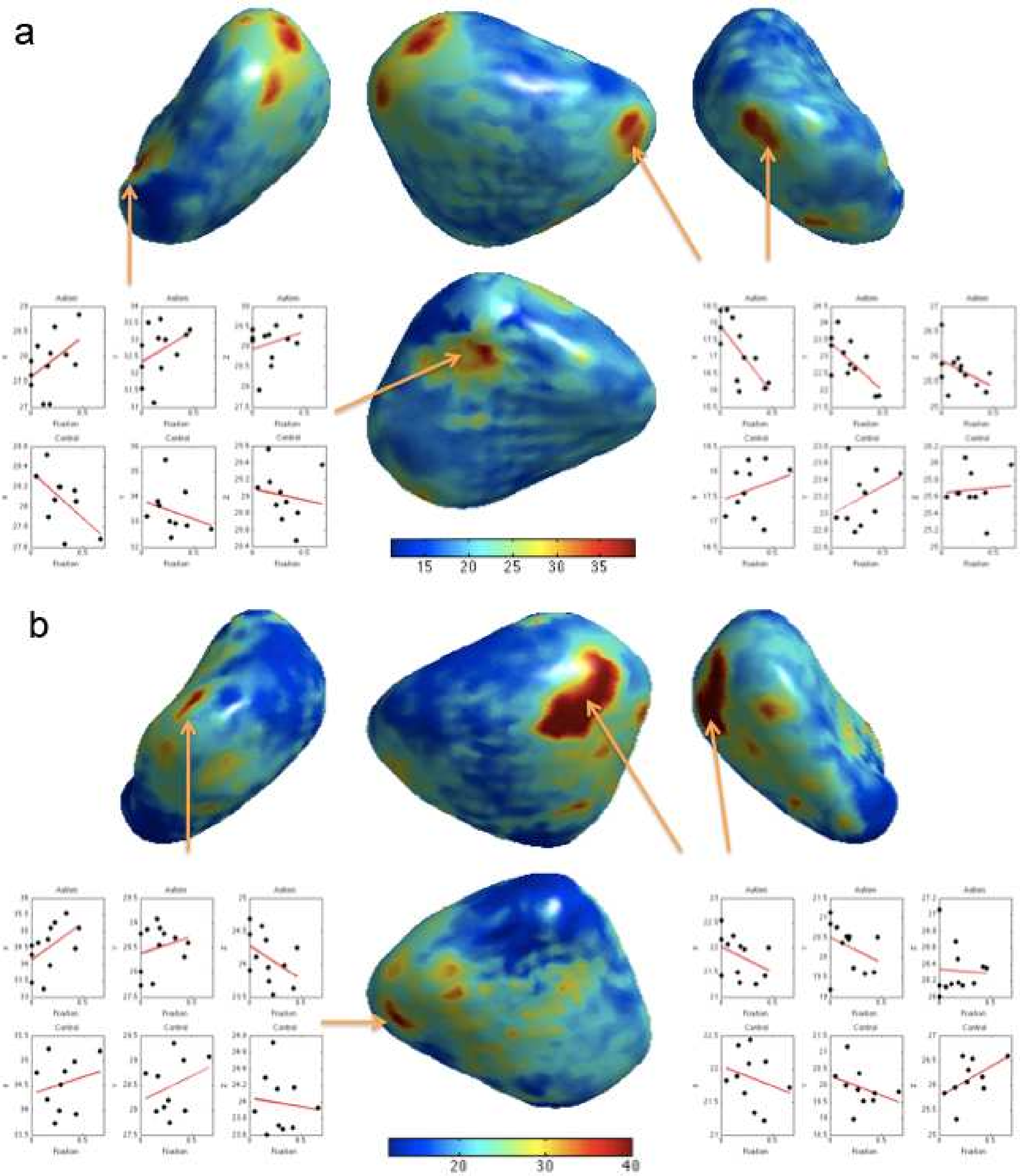

Figure 8. F statistic map of interaction between group and gaze fixation. Red regions show significant interaction. For better visualization, the color bar for the right amygdala (b) has been thresholded at 40 since the maximum F statistics at the largest cluster is 65.68 ($p = 0.003$). Three plots in a row correspond to the scatter plots of x, y and z-coordinates vs. gaze fixation. The first (second) row is for autistic (control) subjects. The red lines are linear regression lines. The significance of interaction implies difference in regression slopes between groups.

7. Conclusions

The paper proposed a unified multivariate linear modeling approach for amygdala shape analysis. The coordinates of amygdala surfaces are smoothed and normalized using the novel weighted spherical harmonic representation. The main methodological contributions are the development of a new amygdala surface flattening technique, the weighted spherical harmonic representation, and AmygSurf and SurfStat packages.

Surface flattening is based on tracing the streamline of the gradient of heat equilibrium. The proposed flattening technique is simple enough to be applied to various applications. Amygdala surfaces are flattened to a sphere to obtain the Euler angle based surface coordinate system. Then the coordinates of amygdala surface meshes are mapped onto a unit sphere to establish the spherical harmonic representation. The representation is used to smooth and to normalize a collection of surfaces. Since the representation is related to heat kernel smoothing, it reduces the Gibbs phenomenon associated with the previous spherical harmonic representation. We have made the whole processing processing and modeling MATLAB pipeline AmygSurf freely available through a website.

Since surface data is inherently multivariate data, traditionally Hotelling's T-square approach has been used on surface coordinates in a group comparison. The proposed multivariate linear model generalizes the Hotelling's T-square approach so that we can construct more complicated statistical models. The model formula based multivariate linear modeling tool SurfStat is also available through a website. We have applied the proposed methods to 22 autistic subjects to test if there is localized shape difference within an amygdala. We were able to localize regions, mainly in the right amygdala, that shows differential association of gaze fixation with anatomy between the groups.

References

Anderson, T. (1984). *An Introduction to Multivariate Statistical Analysis*. Wiley., 2nd. edition.

Angenent, S., Hacker, S., Tannenbaum, A. and Kikinis, R. (1999). On the laplace-beltrami operator and brain surface flattening. *IEEE Transactions on Medical Imaging* **18**, 700–711.

Aylward, E., Minshew, N., Goldstein, G., Honeycutt, N., Augustine, A., Yates, K., Bartra, P. and Pearlson, G. (1999). Mri volumes of amygdala and hippocampus in nonmentally retarded autistic adolescents and adults. *Neurology* **53**, 2145–2150.

Basser, P., Pajevic, S., Pierpaoli, C., Duda, J. and Aldroubi, A. (2000). In vivo tractography using dt-mri data. *Magnetic Resonance in Medicine* **44**, 625–632.

Brechbuhler, C., Gerig, G. and Kubler, O. (1995). Parametrization of closed surfaces for 3d shape description. *Computer Vision and Image Understanding* **61**, 154–170.

Cao, J. and Worsley, K. J. (1999). The detection of local shape changes via the geometry of hotellings t2 fields. *Annals of Statistics* **27**, 925–942.

Chung, M., Dalton, K.M., L. S., Evans, A. and Davidson, R. (2007). Weighted fourier representation and its application to quantifying the amount of gray matter. *IEEE Transactions on Medical Imaging* **26**, 566–581.

Chung, M., Robbins, S., Dalton, K.M., D. R. A. A. and Evans, A. (2005). Cortical thickness analysis in autism with heat kernel smoothing. *NeuroImage* **25**, 1256–1265.

Chung, M., Worsley, K., Paus, T., Cherif, D., Collins, C., Giedd, J., Rapoport, J., and Evans, A. (2001). A unified statistical approach to deformation-based morphometry. *NeuroImage* **14**, 595–606.

Convit, A., McHugh, P., Wolf, O., de Leon, M., Bobinkski, M., De Santi, S., Roche, A. and Tsui, W. (1999). Mri volume of the amygdala: a reliable method allowing separation from the hippocampal formation. *Psychiatry Res.* **90**, 113–123.

Courant, R. and Hilbert, D. (1953). *Methods of Mathematical Physics: Volume II.* Interscience, New York, english edition.

Dalton, K., Nacewicz, B., Johnstone, T., Schaefer, H., Gernsbacher, M., Goldsmith, H., Alexander, A. and Davidson, R. (2005). Gaze fixation and the neural circuitry of face processing in autism. *Nature Neuroscience* **8**, 519–526.

Fischl, B. and Dale, A. (2000). Measuring the thickness of the human cerebral cortex from magnetic resonance images. *PNAS* **97**, 11050–11055.

Foster, J. and Richard, F. (1991). The gibbs phenomenon for piecewise-linear approximation. *The American Mathemtical Monthly* **98**.

Gaser, C., Volz, H.-P., Kiebel, S., Riehemann, S. and Sauer, H. (1999). Detecting structural changes in whole brain based on nonlinear deformationsapplication to schizophrenia research. *NeuroImage* **10**, 107–113.

Gelb, A. (1997). The resolution of the gibbs phenomenon for spherical harmonics. *Mathematics of Computation* **66**, 699–717.

Gerig, G., Styner, M., Jones, D., Weinberger, D. and Lieberman, J. (2001). Shape analysis of brain ventricles using spharm. In *MMBIA*, pages 171–178.

Gerig, G., Styner, M. and Szekely, G. (2004). Statistical shape models for segmentation and structural analysis. In *Proceedings of IEEE International Symposium on Biomedical Imaging (ISBI)*, volume I, pages 467–473.

Gu, X., Wang, Y., Chan, T., Thompson, T. and Yau, S. (2004). Genus zero surface conformal mapping and its application to brain surface mapping. *IEEE Transactions on Medical Imaging* **23**, 1–10.

Haznedar, M., Buchsbaum, M., Wei, T., Hof, P., Cartwright, C. and Bienstock, C.A. Hollander, E. (2000). Limbic circuitry in patients with autism spectrum disorders studied with positron emission tomography and magnetic resonance imaging. *American Journal of Psychiatry* **157**, 1994–2001.

Howard, M., Cowell, P., Boucher, J., Broks, P., Mayes, A., Farrant, A. and Roberts, N. (2000). Convergent neuroanatomical and behavioral evidence of an amygdala hypothesis of autism. *NeuroReport* **11**, 2931–2935.

Hurdal, M. K. and Stephenson, K. (2004). Cortical cartography using the discrete conformal approach of circle packings. *NeuroImage* **23**, S119S128.

Jones, D., Catani, M., Pierpaoli, C., Reeves, S., Shergill, S., O'Sullivan, M., Golesworthy, P., McGuire, P., Horsfield, M., Simmons, A., Williams, S. and Howard, R. (2006). Age effects on diffusion tensor magnetic resonance imaging tractography measures of frontal cortex connections in schizophrenia. *Human Brain Mapping* **27**, 230–238.

Joshi, S. (1998). Large deformation diffeomorphisms and gaussian random fields for statistical characterization of brain sub-manifolds.

Joshi, S., Grenander, U. and Miller, M. (1997). The geometry and shape of brain submanifolds. *International Journal of Pattern Recognition and Artificial Intelligence: Special Issue on Processing of MR Images of the Human* **11**, 1317–1343.

Kelemen, A., Szekely, G. and Gerig, G. (1999). Elastic model-based segmentation of 3-d neuroradiological data sets. *IEEE Transactions on Medical Imaging* **18**, 828–839.

Lazar, M. and Alexander, A. (2003). Lazar, m. and weinstein, d.m. and tsuruda, j.s. and hasan, k.m. and arfanakis, k. and meyerand, m.e. and badie, b. and rowley, h. and haughton, v. and field, a. and witwer, b. and alexander, a.l. *White Matter Tractography Using Tensor Deflection* **18**, 306–321.

Lerch, J. P. and Evans, A. (2005). Cortical thickness analysis examined through power analysis and a population simulation. *NeuroImage* **24**, 163–173.

Lord, C., Rutter, M. and Couteur, A. (1994). Autism diagnostic interviewrevised: a revised version of a diagnostic interview for caregivers of individuals with possible pervasive developmental disorders. *J Autism Dev Disord.* pages 659–685.

Luders, E., Thompson, P.M., Narr, K., Toga, A., Jancke, L. and Gaser, C. (2006). A curvature-based approach to estimate local gyrification on the cortical surface. *NeuroImage* **29**, 1224–1230.

Lundqvist, D., Flykt, A. and Ohman, A. (1998). *Karolinska Directed Emotional Faces.* Department of Neurosciences, Karolinska Hospital, Stockholm, Sweden.

MacDonald, J., Kabani, N., Avis, D. and Evans, A. (2000). Automated 3-D extraction of inner and outer surfaces of cerebral cortex from mri. *NeuroImage* **12**, 340–356.

Mai, J., Assheuer, J. and Paxinos, G. (1997). *Atlas of the Human Brain.* Academic Press, San Diego.

Miller, M., Massie, A., Ratnanather, J., Botteron, K. and Csernansky, J. (2000). Bayesian construction of geometrically based cortical thickness metrics. *NeuroImage* **12**, 676–687.

Nacewicz, B., Dalton, K., Johnstone, T., Long, M., McAuliff, E., Oakes, T., Alexander, A. and Davidson, R. (2006). Amygdala volume and nonverbal social impairment in adolescent and adult males with autism. *Arch. Gen. Psychiatry* **63**, 1417–1428.

Pierce, K., Muller, R.A., A. J., Allen, G. and Courchesne, E. (2001). Face processing occurs outside the fusiform "face area" in autism: evidence from functional mri. *Brain* **124**, 2059–2073.

Qiu, A., and Miller, M. (2008). Multi-structure network shape analysis via normal surface momentum maps. *NeuroImage* **42**, 1430–1438.

Rojas, D., Smith, J., Benkers, T., Camou, S., Reite, M. and Rogers, S. (2000). Hippocampus and amygdala volumes in paretns of children with autistic disorder. *The Canadian Journal of Statistics* **28**, 225–240.

Roy, S. (1953). On a heuristic method of test construction and its use in multivariate analysis. *Ann. Math. Statist.* **24**, 220–238.

Schumann, C., Hamstra, J., Goodlin-Jones, B., Lotspeich, L., Kwon, H., Buonocore, M., Lammers, C., Reiss, A. and Amaral, D. (2004). The amygdala is enlarged in children but not adolescents with autism; the hippocampus is enlarged at all ages. *Journal of Neuroscience* **24**, 6392–6401.

Sethian, J. (2002). *Level Set Methods and Fast Marching Methods: Evolving Interfaces in Computational Geometry, Fluid Mechanics, Computer Vision and Material Science.* Cambridge University Press.

Shen, L. and Chung, M. (2006). Large-scale modeling of parametric surfaces using spherical harmonics. In *Third International Symposium on 3D Data Processing, Visualization and Transmission (3DPVT)*.

Shen, L., Ford, J., Makedon, F. and Saykin, A. (2004). surface-based approach for classification of 3d neuroanatomical structures. *Intelligent Data Analysis* **8**, 519–542.

Sparks, B., Friedman, S., Shaw, D., Aylward, E., Echelard, D., Artru, A., Maravilla, K., Giedd, J., Munson, J., Dawson, G. and Dager, S. (2002). Brain structural abnormalities in young children with autism spectrum disorder. *Neurology* **59**, 184–192.

Taylor, J. and Worsley, K. (2008). Random fields of multivariate test statistics, with applications to shape analysispage in press.

Thompson, P. and Toga, A. (1996). A surface-based technique for warping 3-dimensional images of the brain. *IEEE Transactions on Medical Imaging* **15**.

Thompson, P. M., MacDonald, D., Mega, M. S., Holmes, C. J., Evans, A. C. and Toga, A. W. (1997). Detection and mapping of abnormal brain structure with a probabilistic atlas of cortical surfaces. *J. Comput. Assist. Tomogr.* **21**, 567–581.

Timsari, B. and Leahy, R. (2000). An optimization method for creating semi-isometric flat maps of the cerebral cortex. In *The Proceedings of SPIE, Medical Imaging*.

Worsley, K., Marrett, S., Neelin, P., Vandal, A., Friston, K. and Evans, A. (1996). A unified statistical approach for determining significant signals in images of cerebral activation. *Human Brain Mapping* **4**, 58–73.

Worsley, K., Taylor, J., Tomaiuolo, F. and Lerch, J. (2004). Unified univariate and multivariate random field theory. *NeuroImage* **23**, S189–195.